NASA TECHNICAL NOTE

NASA TN D-4321

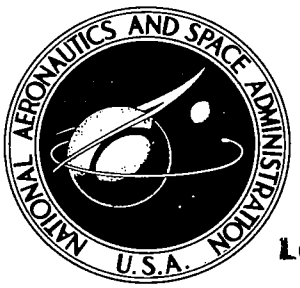

NASA TN D-4321

FLUTTER OF CORRUGATION-STIFFENED PANELS AT MACH 3 AND COMPARISON WITH THEORY

by Herman L. Bohon

Langley Research Center
Langley Station, Hampton, Va.

NATIONAL AERONAUTICS AND SPACE ADMINISTRATION • WASHINGTON, D. C. • MARCH 1968

FLUTTER OF CORRUGATION-STIFFENED PANELS AT MACH 3 AND COMPARISON WITH THEORY

By Herman L. Bohon

Langley Research Center
Langley Station, Hampton, Va.

NATIONAL AERONAUTICS AND SPACE ADMINISTRATION

For sale by the Clearinghouse for Federal Scientific and Technical Information
Springfield, Virginia 22151 – CFSTI price $3.00

FLUTTER OF CORRUGATION-STIFFENED PANELS AT MACH 3 AND COMPARISON WITH THEORY

By Herman L. Bohon
Langley Research Center

SUMMARY

Details of an experimental study on flutter of corrugation-stiffened panels are presented. The panels were tested at Mach 3 in the Langley 9- by 6-foot thermal structures tunnel under aerodynamic heating conditions. Flutter boundaries presented include a flat-panel portion and a thermally buckled panel portion. Comparison of the results from this investigation and other available data on corrugation-stiffened panels with conventional theory for panels simply supported on all edges indicates that theory is highly unconservative. However, accounting in the theory for the deflectional flexibility of the corrugations and supports at the ends of the corrugations brings theory and experiment into fair agreement. These results indicate that seemingly small details of edge conditions of corrugation-stiffened panels may cause drastic reductions in the dynamic pressure for flutter.

INTRODUCTION

In the past few years, considerable research has been conducted on the flutter of isotropic panels; however, until recently, little effort has been directed toward the complex orthotropic panel. Nevertheless, orthotropic panels (generally corrugation stiffened) have had widespread application in design of high supersonic and reentry type vehicles and, in fact, flutter of such panels has occurred in flight. (See, for example, ref. 1.) Thus, the prediction of flutter may be significant in the design of orthotropic panels.

The comparison of experimental flutter data for corrugation-stiffened panels with results from conventional theory indicates theoretical predictions are highly unconservative. This result has been illustrated in reference 2 where the comparison of experimental results with results obtained from theory resulted in poor agreement unless measured frequencies and mode shapes were employed in the theory. Similarly, in reference 3 the use of conventional theory resulted in predicted critical dynamic pressures over an order of magnitude greater than those obtained experimentally. In this reference the discrepancy was attributed to the fact that finite deflectional flexibility of the panel at the ends of the corrugations was not accounted for in the theory. An approximate flutter

analysis presented in reference 4 verified that details of boundary conditions at the panel edges normal to the direction of maximum flexural stiffness have a large influence on panel flutter behavior. A more exact theoretical analysis is presented in reference 5 where exact vibration mode shapes and frequencies are employed for arbitrary deflectional stiffness of the supports. Comparisons of these theoretical results with experimental results showed reasonable agreement.

In the present report additional experimental data on the flutter of corrugation-stiffened panels are presented. The panels were elastically restrained along the edges to permit both in-plane and rotational displacements. The panels were tested with the corrugations alined normal to the stream in the Langley 9- by 6-foot thermal structures tunnel, a Mach 3 blowdown facility, at dynamic pressures ranging from 1500 psf to 5000 psf (72 to 239 kN/m^2) and stagnation temperatures from 350° F to 660° F (450° to 620° K).

The deflectional stiffnesses of the supports were calculated by making certain structural idealizations; details of these calculations are presented in appendix A. With the use of these deflectional stiffnesses, the experimental data of this investigation and flutter data on corrugation-stiffened panels from other recent investigations are compared with results obtained from the theory of reference 5.

SYMBOLS

The units used for the physical quantities in this paper are given both in the U.S. Customary Units and in the International System of Units (SI). Factors relating the two systems are given in reference 6 and those used in the present investigation are presented in appendix B.

a length of panel

b width of panel

c,d,e,f,g,i,j,s,r_1,r_2 dimensions of corrugations and edge attachments (see fig. 10)

D_1 flexural stiffness of panel in stream direction

D_2 flexural stiffness of panel in cross-stream direction

D_{12} twisting stiffness of panel

E Young's modulus

f	panel natural frequency
f_f	panel vibration frequency at flutter
K, K_1, K_2	equivalent spring stiffnesses of panel (see appendix A)
$\overline{K}$	deflectional stiffness parameter, $\frac{Kb^3}{\pi^3 D_2}$
m	integer describing number of half-waves in mode shape
M	Mach number
Δp	differential pressure (positive when pressure behind the panel exceeds free-stream pressure)
q	dynamic pressure
t	time
t_a	thickness of angle support
t_c	thickness of corrugation sheet
t_s	thickness of cover sheet
T_t	stagnation temperature
T	panel temperature
ΔT_1	average change in temperature of cover sheet
ΔT_2	average change in temperature of cover sheet and corrugation
ΔT_3	average change in temperature of bottom of corrugation

$\beta = \sqrt{M^2 - 1}$

θ angle of corrugation (see fig. 10)

λ dynamic pressure parameter, $\frac{2qa^3}{\beta D_1}$

λ_{cr} experimental value of dynamic pressure parameter at flutter

λ_{th} theoretical value of dynamic pressure parameter at flutter

$\lambda_{\overline{K}=\infty}$ theoretical value of dynamic pressure parameter at flutter for simply supported panel

TESTS

Panels

Each panel consisted of a flat outer skin, seam welded to a sheet of preformed corrugations alined normal to the airstream. Three types of panels were tested. Pertinent construction details are given in figure 1. One type of panel (designated panel III), made of René 41, 23.82 inches (60.5 cm) square, had U-shaped corrugations that were 0.38 inch deep and 0.52 inch wide (0.97 by 1.32 cm). The other two types of panels (designated panels IV and V) made of 301 stainless steel, had square-shaped corrugations 0.50 inch deep and 0.50 inch wide (1.27 by 1.27 cm). Panel IV was 19.00 inches (48.2 cm) square, and panel V was 23.82 inches (60.5 cm) square. The panels were supported along the edges by formed channel sections 1.680 inches (4.27 cm) deep, which were attached to the skin by riveting. The channels at the leading and trailing edges were 0.062 inch (0.158 cm) thick and the channels along the sides were 0.025 inch (0.064 cm) thick. In addition, the panels were supported at the ends of the corrugations by angle clips riveted to the channels running along the length of the panels.

Test Apparatus

Tunnel.- The tests were made at Mach 3 in the Langley 9- by 6-foot thermal structures tunnel, a blowdown facility exhausting to the atmosphere and capable of stagnation temperatures up to 660° F (623° K). For details regarding the tunnel and its operation, see reference 7.

Panel holder and mounting arrangement.- The panels were mounted in a flat-sided steel panel holder having a beveled half-wedge leading edge and extending vertically through the test section. (See fig. 2.) A cavity 29 inches (74 cm) in the direction of flow and 30 inches (76 cm) high is located 27 inches (68 cm) downstream of the leading edge on the nonbeveled surface of the panel holder. The panel holder is equipped with

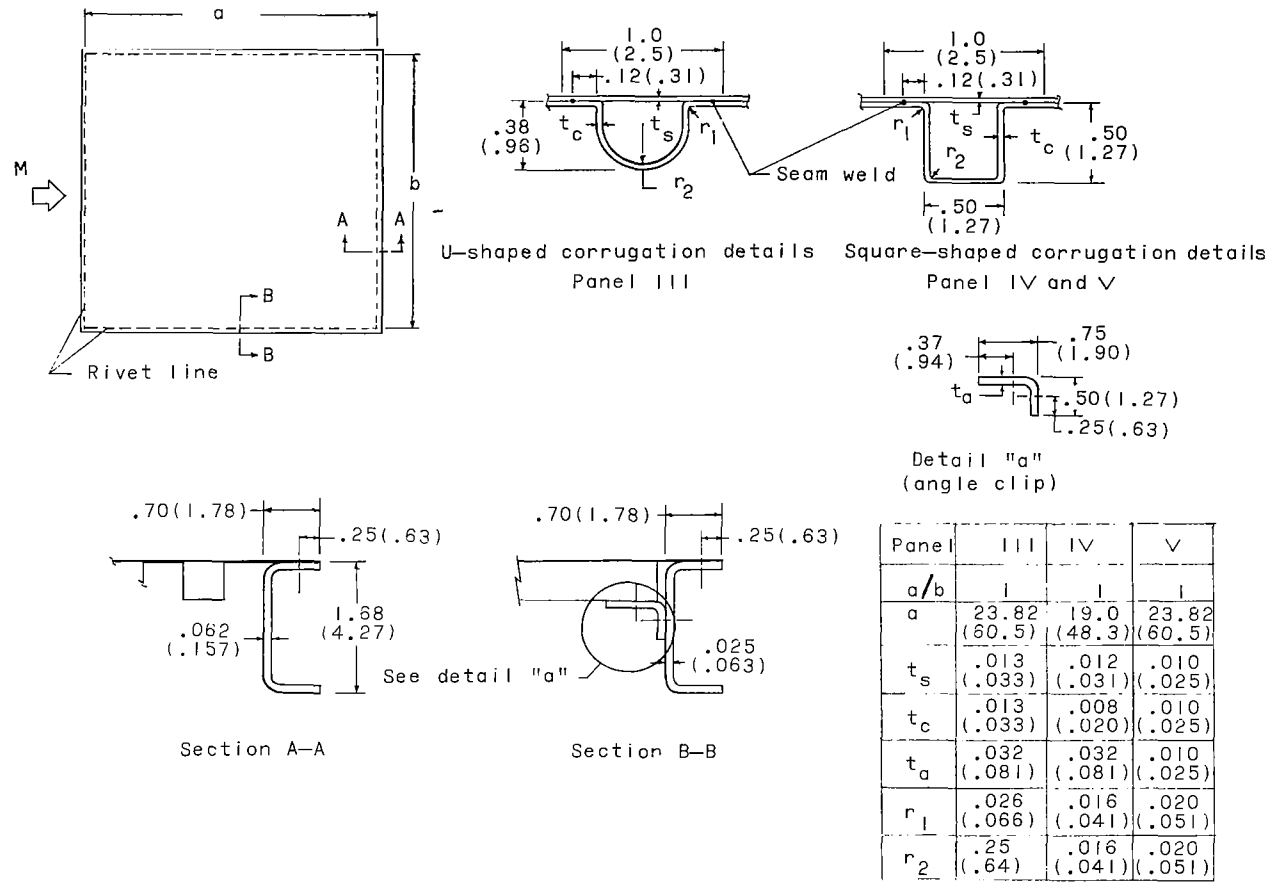

Panel	III	IV	V
a/b	1	1	1
a	23.82 (60.5)	19.0 (48.3)	23.82 (60.5)
t_s	.013 (.033)	.012 (.031)	.010 (.025)
t_c	.013 (.033)	.008 (.020)	.010 (.025)
t_a	.032 (.081)	.032 (.081)	.010 (.025)
r_1	.026 (.066)	.016 (.041)	.020 (.051)
r_2	.25 (.64)	.016 (.041)	.020 (.051)

Figure 1.- Panel construction details. All dimensions are in inches (centimeters).

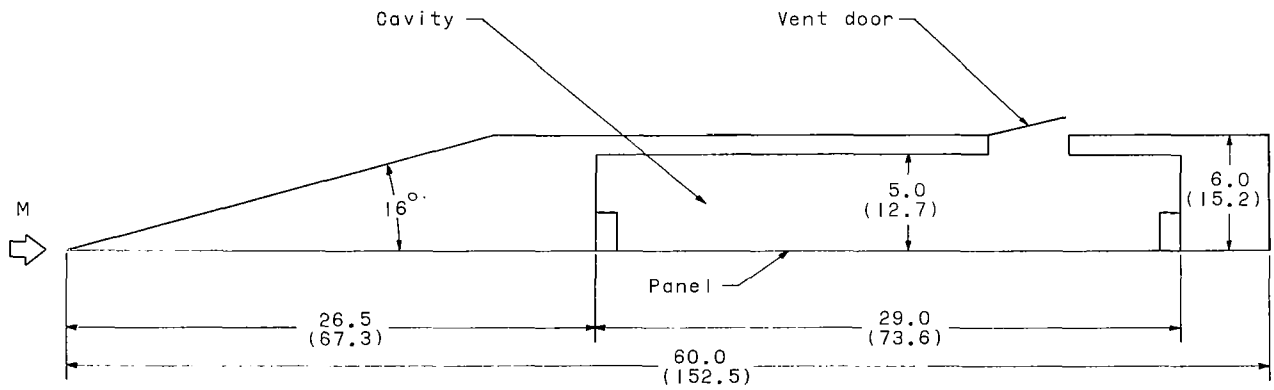

Figure 2.- Cross section of panel holder. All dimensions are in inches (centimeters).

pneumatic, vertically operating sliding doors which cover the cavity area for protection of test specimens during tunnel start and shutdown. Aerodynamic fences attached to the doors insure essentially free-stream flow conditions over the cavity area. (See ref. 7.) The pressure inside the cavity and behind a test specimen is controlled by a vent-door arrangement on the side of the panel holder opposite the panel. The test panels were assembled to a mounting frame, which was inserted in the cavity so that the surface of the panel was flush with the surface of the panel holder. The rectangular mounting frame and panel assembly used for panels III and V is shown in figure 3, and the disk-type mounting frame used for panel IV is shown in figure 4.

Attachment of a panel to the mounting frame was accomplished by bolting the bottom legs of the formed channel section (along the edges of the panel skin) to a flat aluminum plate which, in turn, was attached to the steel angle-section mounting frame. (See fig. 5.) The combination was then inserted in the cavity in the panel holder, as previously described, with the corrugations alined perpendicular to the direction of airflow. This mounting arrangement permitted partial thermal expansion of the panel skin in both the longitudinal and lateral direction by flexure of the channel section.

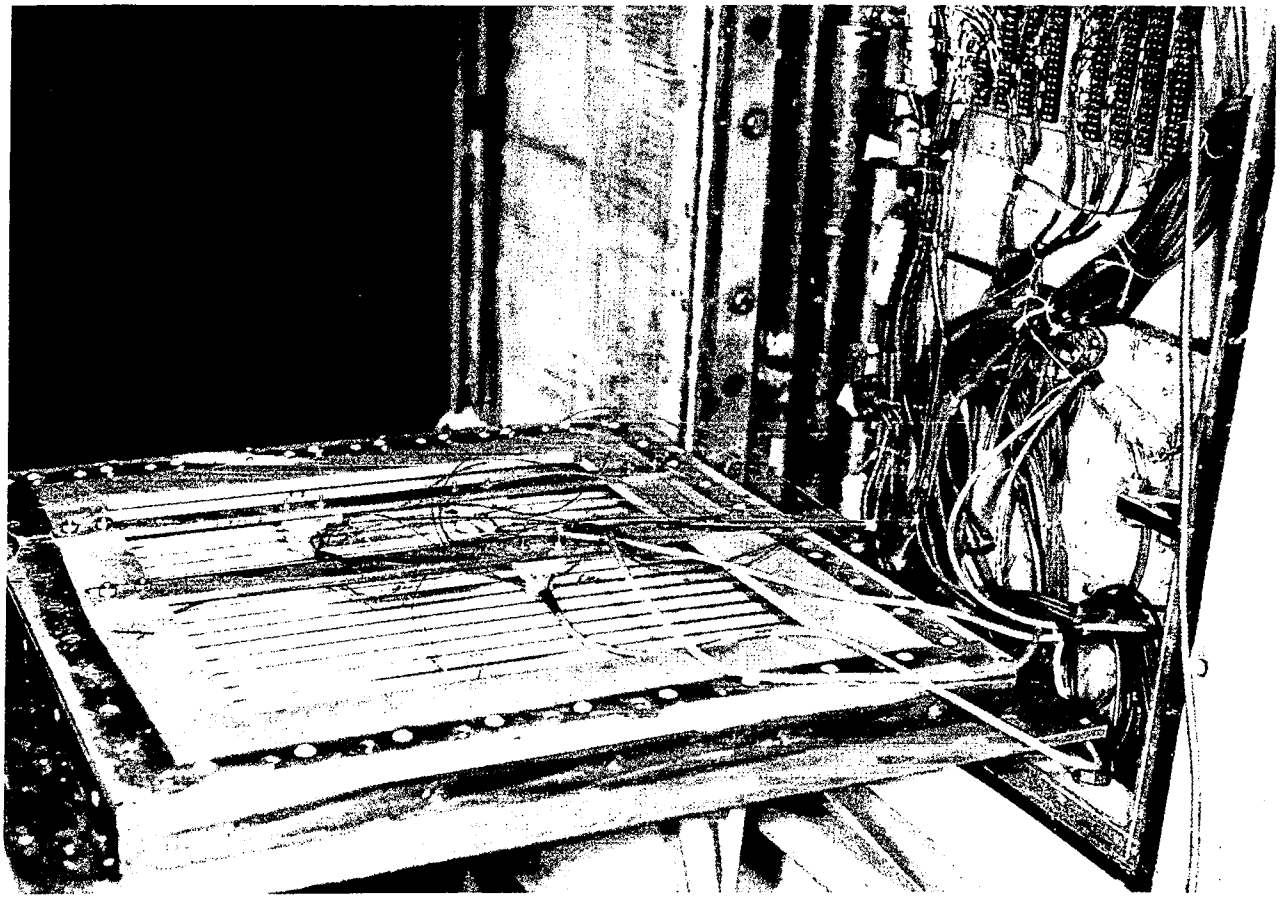

Figure 3.- View of rear of assembled panel III and rectangular mounting frame ready to insert in panel holder. L-61-4105

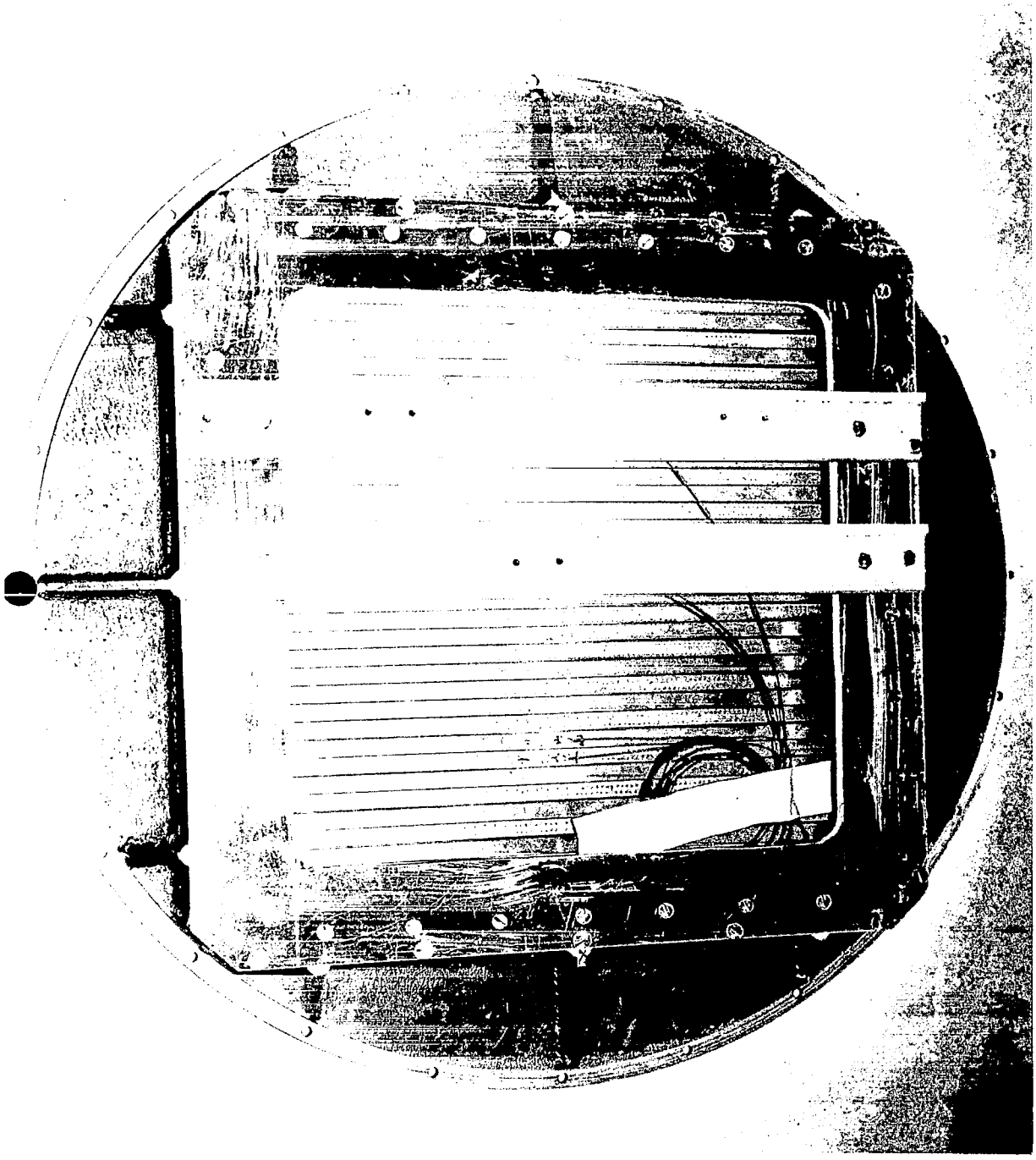

Figure 4.- Rear view of panel IV showing disk-type mounting frame and deflectometer supports. L-62-3893

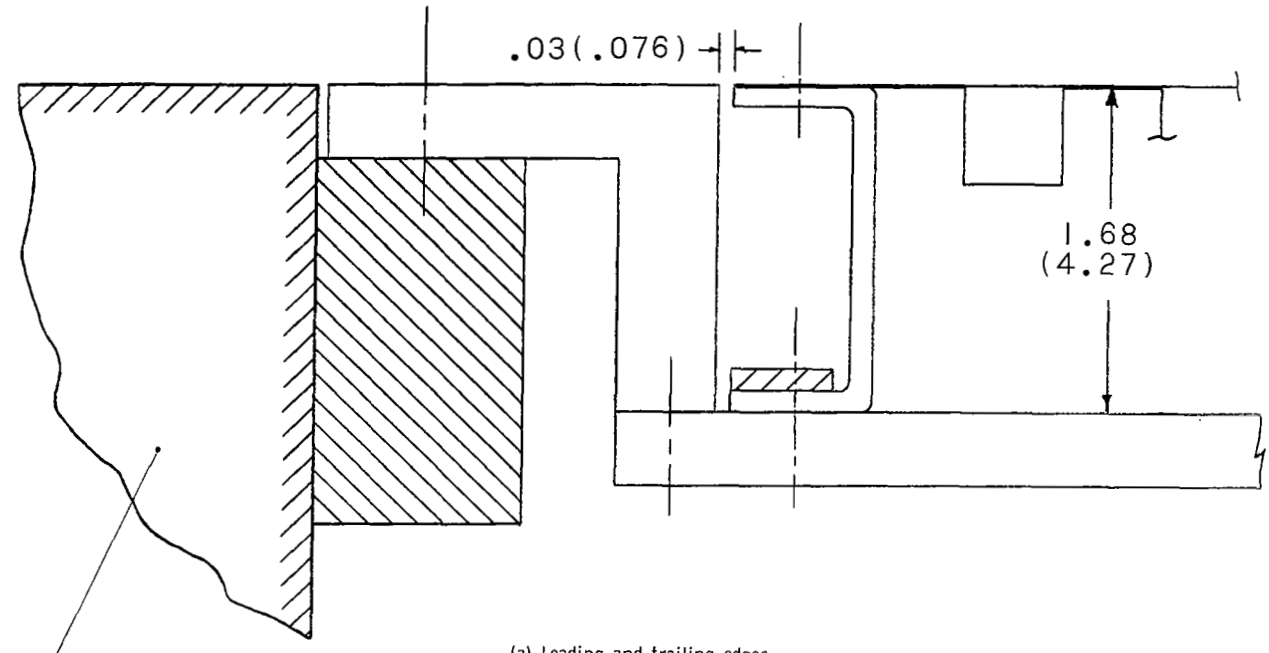

(a) Leading and trailing edges.

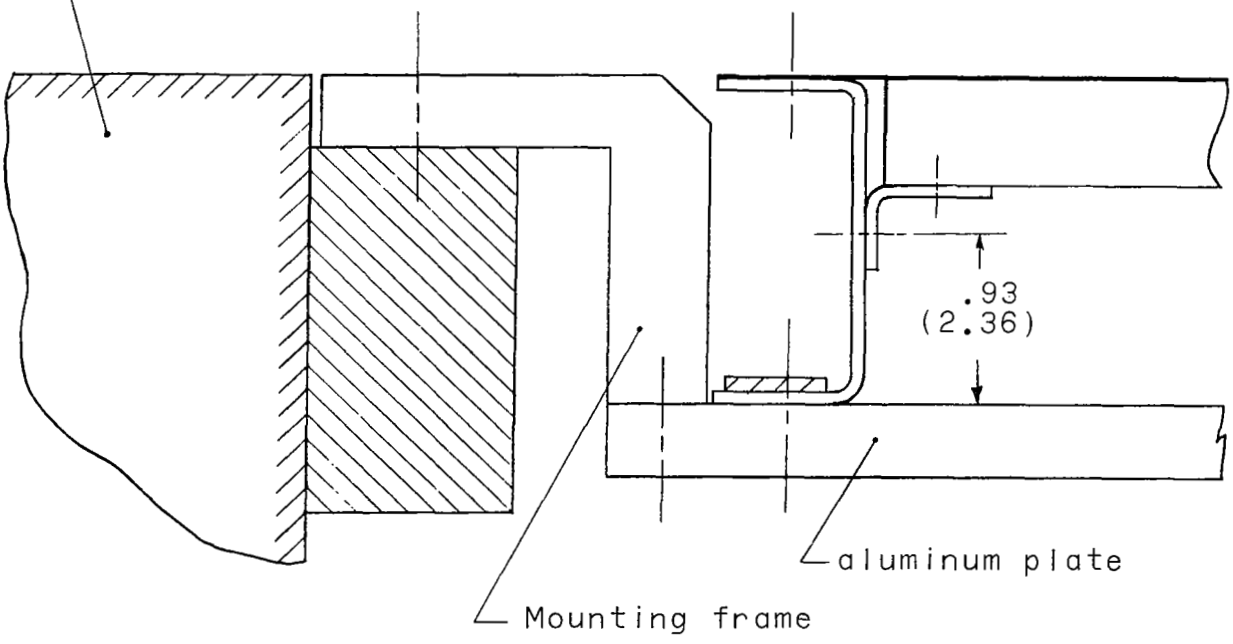

(b) Longitudinal edges.

Figure 5.- Panel mounting arrangement. All dimensions are in inches (centimeters).

Instrumentation

Panel instrumentation consisted of thermocouples and deflectometers, supplemented by motion pictures. Thirteen iron-constantan thermocouples were spotwelded to each of panels III and V at the locations shown in figure 6 in order to obtain an approximate survey of the temperatures experienced during a test. Panel IV was instrumented with thermocouples 1 and 2, 4 and 5, and 8 spaced at 5-inch (12.7 cm) intervals along the panel center line. Three variable reluctance-type deflectometers located 3/4 inch (1.90 cm) from the corrugations were used (see fig. 6) to detect panel motion and to obtain flutter frequencies. Additional data on panel behavior were obtained with high-speed 16-millimeter motion pictures taken at speeds up to 2000 frames per second. The exposed surface of the panel was painted with a grid to facilitate visual detection of panel motion.

Static pressures in the tunnel and static pressures at several locations on the panel holder and also in the cavity behind the panels were measured by quick-response, strain-gage-type pressure transducers. Tunnel stagnation pressures were obtained from static pressures measured in the settling chamber. Stagnation temperatures were measured by total-temperature probes in the test section. All pressure and temperature data were recorded on magnetic tape; deflectometer output, which was monitored during each test, was recorded on oscillographs.

Test Procedure

All tests were conducted at a Mach number of 3.0, at dynamic pressures from 1500 psf (72 kN/m^2) to 5000 psf (239 kN/m^2) and at stagnation temperatures between 350° F (450° K) and 600° F (590° K). During a test the stagnation temperature was maintained essentially constant, whereas the dynamic pressure, although usually held constant, was varied in some tests. The usual test procedure was to establish test conditions and then expose the panel to the airflow at constant dynamic pressure. These conditions were maintained until the thermal stresses resulting from the aerodynamic heating increased sufficiently to initiate flutter, then the protective doors were closed, and the test terminated. For some tests, however, after flutter had been initiated, the dynamic pressure was decreased in an effort to stop flutter, and then sometimes the pressure was increased to restart flutter. The duration of a test was from 15 to 45 seconds.

RESULTS AND DISCUSSION

Seven tests were made on panel III, five tests on panel IV, and three tests on panel V. Two panels were tested for each of panel types III and IV. All tunnel and panel conditions recorded for each flutter start and stop point are given in table I. The data tabulated are the stagnation temperature T_t, the dynamic pressure q, the differential

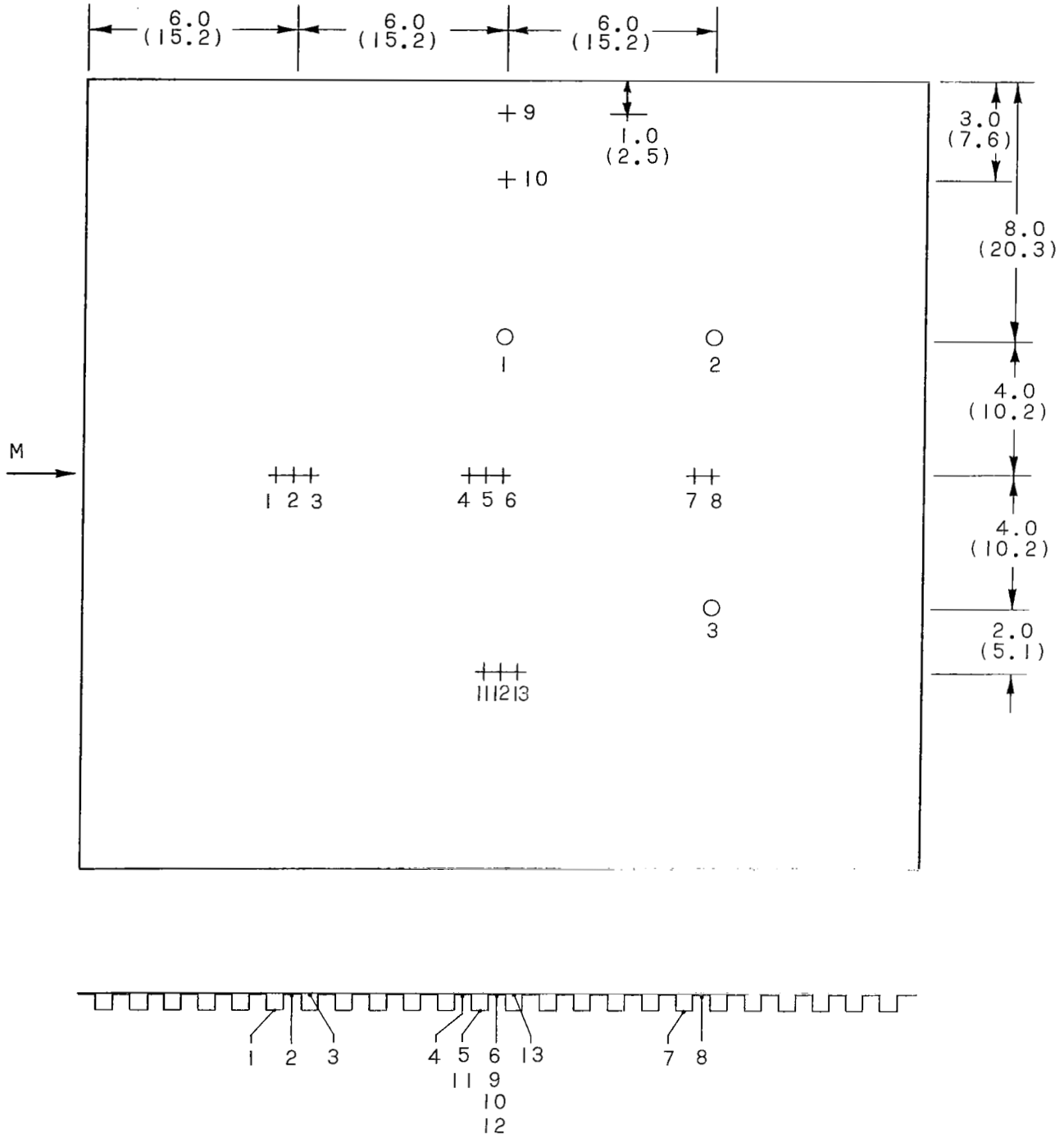

Figure 6.- Instrumentation details. All dimensions are in inches (centimeters).

pressure between the two faces of the panel Δp, the average temperature increases of the cover sheet ΔT_1, the double thickness of cover sheet and corrugated sheet ΔT_2, and the bottom of the corrugations ΔT_3. The temperature increases are averages of corresponding thermocouples shown in figure 6. All temperature readings were within ±5 percent of the average. Also tabulated are the panel frequencies at the inception and termination of flutter f_f.

Flutter Test Data

During a test the dynamic pressure and panel temperature were the primary variables. The dynamic pressure was controlled manually whereas the panel temperature varied as a result of aerodynamic heating. Although the temperature varied through the panel (see table I), no attempt was made to convert these gradients to thermal stress. Also, the panel differential pressure was intended to be maintained at zero, but limitations on the manual controls resulted in differential pressure readings that generally differed for each flutter point. These variables no doubt contributed to scatter in the test results, but were neglected in the reduction and correlation of data.

A trace of the test variables is shown in figure 7 for test 4 on panel IVb. Figure 7(a) is a plot of the panel temperature variation during the test, based on the average of the readings of thermocouples 2, 4, and 8 at the double sheet thickness and the average of thermocouples 1 and 5 at the bottom of the corrugations. (See fig. 6.) Note during the first 2.5 seconds of the test the protective doors, covering the panel from the airstream, permitted very little change in the panel temperature. Figure 7(b) is a trace of the variable dynamic pressure for the same test in which flutter was started and stopped several times. After the protective doors were opened (2.5 sec), the dynamic pressure was maintained essentially constant whereas thermal stresses increased sufficiently to cause flutter. The flutter initiated was termed large amplitude (represented by the solid band) in that the sudden growth of deflection indicated by the deflectometer output was several times the panel skin thickness; also the fluttering motion was readily distinguished from observation of the high-speed movies. As indicated in figure 7(b), once flutter was initiated, the dynamic pressure was decreased until flutter ceased (indicated by the termination of the solid band). Note from figure 7(a) that the panel temperature is also changing. Flutter was again initiated and terminated by increasing the dynamic pressure as indicated by the solid band at 17.2 seconds and then decreasing the pressure until flutter stopped. This procedure of varying the dynamic pressure was repeated to get other flutter start and stop points at other temperature levels.

When flutter start points were obtained, the panel was flat except as denoted in table I. Also, at the end of flutter the panels were observed from the motion-picture film to be in a thermally buckled state except as denoted in table I. The initiation of

large-amplitude flutter of the thermally buckled panel was generally preceded by a short period (approximately 1 sec) of small-amplitude perturbation about the buckled shape.

Observation of the high-speed motion-picture film revealed that fluttering motion was generally of the standing wave type, and the large-amplitude motion was pronounced near the trailing edge. Panel IV, however, occasionally fluttered in a mode with several half-waves in the stream direction. All fluttering motion was verified by visual observation of the high-speed film.

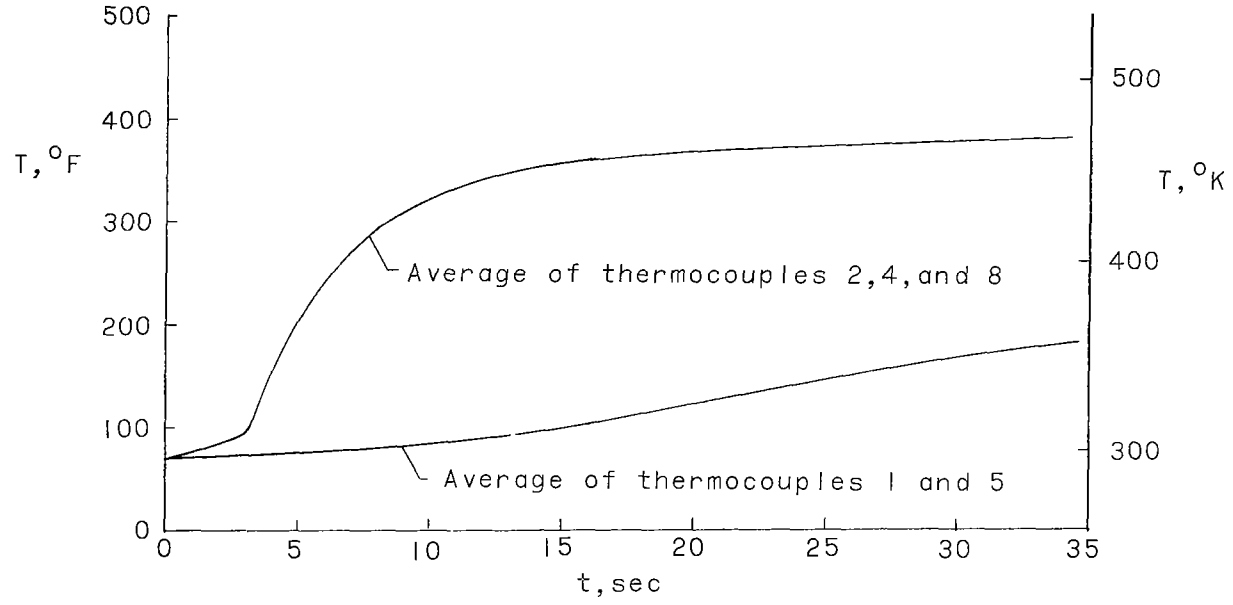

(a) Temperature variation due to aerodynamic heating.

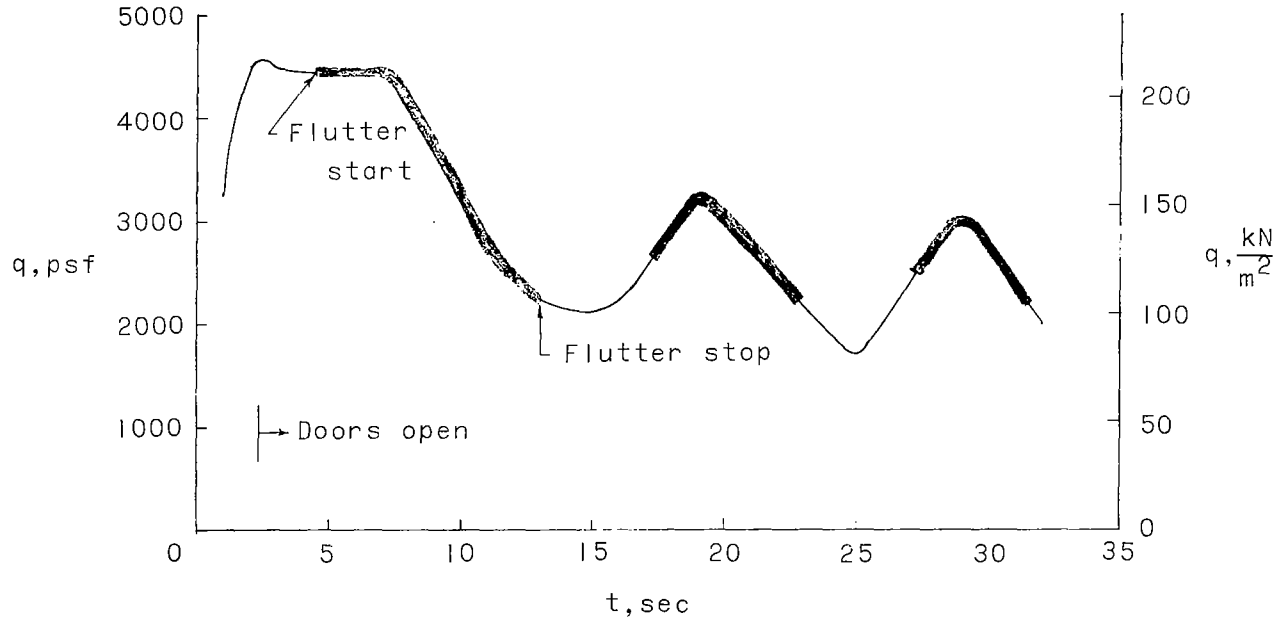

(b) Dynamic-pressure variation showing periods of flutter.

Figure 7.- Test variable histories and periods of flutter. Panel IVb; test 4.

Flutter Boundaries

The flutter points from all tests are shown in figure 8 on plots of the dynamic pressure and panel temperature increase ΔT_2. The open and solid symbols correspond to the initiation of flutter for the panel in a flat condition or buckled condition, respectively. The flagged symbols represent the termination of flutter. The curves through the points represent the experimental flutter boundaries for panel III (fig. 8(a)), panel IV (fig. 8(b)), and panel V (fig. 8(c)). With the exception of the data from panel V, the boundaries consist of a flat-panel portion and a buckled-panel portion. The minimum tunnel conditions (1500 psf) (72 kN/m^2) would not permit determination of the minimum dynamic pressure for panel V (fig. 8(c)). The "no flutter" test shown by the dashed curve in figure 8(a) was conducted at constant dynamic pressure in order to aid in the determination of the minimum dynamic pressure for which flutter could be induced.

The effect of aerodynamic heating on flutter of corrugation-stiffened panels is evident from the boundaries shown in figure 8. For the flat panel, as the stress due to aerodynamic heating increases, the dynamic pressure required for flutter decreases; this trend is generally reversed once the panel is buckled. The flat-panel flutter boundaries are extrapolated to zero stress (zero temperature increase) to determine the corresponding dynamic pressure for flutter for use in the comparison with theory.

No attempt is made to compare the stressed panel boundary with theory since the evaluation of thermal stresses of the panels would be very approximate at best. The slope of theoretical boundaries for flat stressed panels is strongly dependent on stress ratio (see, for example, ref. 8) and, in addition, reference 9 has shown the degree of rotational restraint to have a large influence on flutter when the panel is stressed near the point of buckling. However, neither of these effects has an appreciable influence on the flutter dynamic pressure at zero stress for highly orthotropic panels. It is apparent from the limited scatter of the data of figure 8 that the neglect of Δp variation and temperature variation through the panel also had little effect on the zero stress point.

COMPARISON OF THEORY AND EXPERIMENT

The theory of reference 5 has been applied to the experimental flutter data for the three panels of the present investigation and for several other corrugation-stiffened panels from references 3, 10, 11, and 12. The theory corresponds to simply supported leading and trailing edges and zero moment but finite deflectional restraint along the side edges. In the application of the theory it is necessary to specify the panel geometry, bending and twisting stiffnesses, and the equivalent deflectional spring stiffness of the edge supports. These data are given in table II.

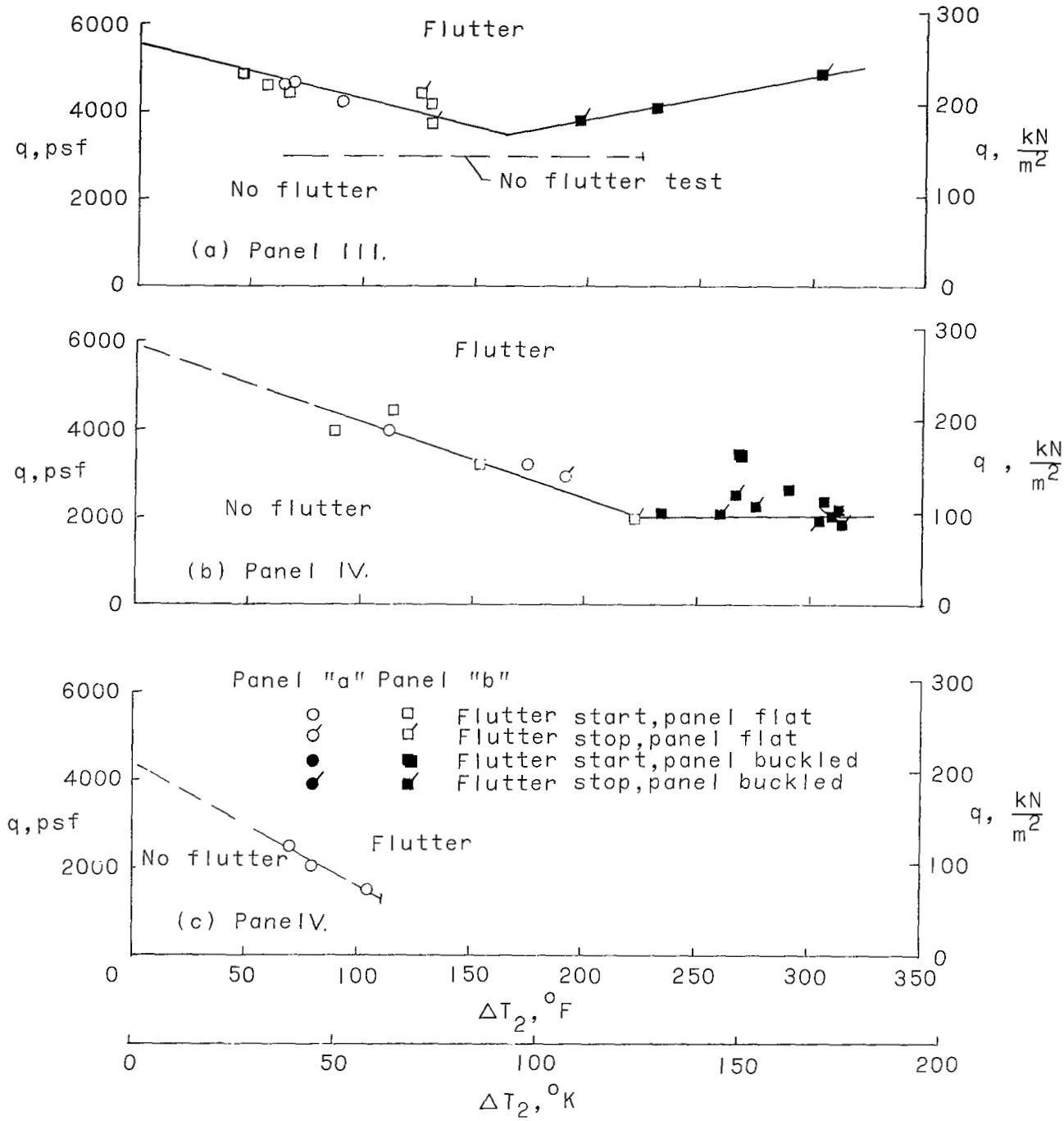

Figure 8.- Flutter boundaries for corrugation-stiffened test panels as result of thermal stress.

Details of the calculations of spring stiffness K are given in appendix A for each of the four support types listed. In some cases the edge flexibility came from two

sources as indicated by the separate spring constants K_1 and K_2 which are added in series $\left(\frac{1}{K} = \frac{1}{K_1} + \frac{1}{K_2}\right)$ to obtain the total spring constant. The nondimensional spring stiffness parameter $\overline{K} = Kb^3/\pi^3 D_2$ used in reference 5 is also shown. Also listed in table II is Young's modulus E, and the flexural stiffnesses D_1 and D_2 and twisting stiffness D_{12}.

The stiffnesses listed in reference 12 (in errata) for the panels therein differ somewhat from those tabulated in this report; these differences may be attributed to slight variations in the treatment of geometric details of the corrugations as well as minor differences in the methods employed to calculate the stiffnesses. The method used for all the panels herein is presented in reference 13.

Experimental values of the critical dynamic pressure parameter $\lambda_{cr}\left(\lambda = \frac{2qa^3}{\beta D_1}\right)$ corresponding to zero stress values are compared with theory in table III. Some of the panels of reference 12 experienced flutter at several Mach numbers and resulted in different values of λ_{cr}. For these panels the Mach number listed in table III corresponds to the test which produced the lowest value of λ_{cr}.

The critical values of the dynamic pressure parameter from theory (λ_{th}) were obtained from reference 5 by using the calculated values of deflectional stiffness $\overline{K}$ and up to 18 modes in the analysis. The number of modes necessary for convergence increases with the degree of orthotropy (ref. 14) and converged results could not be obtained by direct calculations for all the panels listed in table III, even by using 18 modes. For such panels the method suggested in reference 5 was used and consists of determining the variation of the dynamic pressure q with panel length-width ratio to find the value wherein the dynamic pressure is independent of panel length. This converged value is then used in an extrapolation to the length-width ratio of the panel in question. Thus, the theoretical assessments of the panels, shown in table III as a ratio of theory to experiment, are believed to be accurate within the realm of the calculated stiffnesses used in the analysis. As can be seen from the table, some theoretical predictions differ by as much as a factor of 3 on either side of experiment, most predictions being within a factor of 2. It should be noted, however, that this comparison is in terms of the critical dynamic pressure q; a comparison in terms of panel material thickness would result in values less than the cube root of the ratio $\lambda_{th}/\lambda_{cr}$.

Panels I and II from reference 3 are nominally identical to panels U-2 and H-1, respectively, from reference 12, but differed in their method of support. The panels from reference 3 were attached to a flexure-type support along the bottom of the corrugations and the major contribution to calculated value of $\overline{K}$ resulted from a distortion of the corrugations. (See appendix A.) Panels U-2 and H-1 were supported by the cover sheet material only and the corrugated sheet was unsupported. Thus, the supports of the

panels of reference 12 were considerably weaker than those of the identical panels of reference 3. This difference in support attachment resulted in a marked reduction in the critical dynamic pressure as is apparent when values of λ_{cr} from table III are compared.

Also shown in table III as the ratio $\lambda_{\overline{K}=\infty}/\lambda_{cr}$ are theoretical values of the dynamic pressure parameter from an exact analysis (ref. 5) for springs of infinite stiffness (unyielding supports). These latter values ($K = \infty$) are shown since they constitute the upper limit of the dynamic pressure parameter for unyielding supports. The very large effect (over three orders of magnitude decrease in dynamic pressure) of finite support deflection is immediately obvious and if attention is given to methods of attaching corrugation-stiffened panels to the substructure to reduce support flexibility, large increases in the dynamic pressure for flutter may be realized. The salient fact is that local distortions of the corrugation cross section and attachments are very significant in reducing the deflectional stiffness at the supports. Properly accounting for these distortions appears to remove the greater part of the discrepancy between theory and experiment. It is believed that the remaining differences between theory and experiment reflect possible inadequacy in calculated panel stiffnesses and deflectional spring stiffnesses. Such a conjecture may be verified, however, only by a carefully controlled experimental investigation.

The validity of the calculations of the deflectional spring stiffnesses is strengthened somewhat by the results shown in figure 9 where the measured frequencies of one of the test panels are compared with the theoretical frequencies. The first five measured natural frequencies of panel I are shown by the circles in figure 9. (Higher mode frequencies were not obtained during the investigation.) The theoretical curves are obtained from reference 5 where the leading and trailing edges are treated as simply supported and the lateral edges have either zero slope (solid lines) or zero moment (dashed lines). The calculated value of the deflectional stiffness parameter $\overline{K}$ for panel I is 63 (see table III), and the corresponding theoretical curves for zero slope and for zero moment are so labeled on the figure. The curves for infinite spring stiffness $\left(\overline{K} = \infty\right)$ illustrate the magnitude of the effect of support flexibility on the panel frequencies. As can be seen from figure 9, the theoretical curve for $\overline{K} = 63$ and zero moment closely predicts the measured frequencies and has the same trend as the experiment especially at the higher modes. A better assessment of the value of $\overline{K}$ could possibly be made if higher mode frequencies had been obtained.

It is significant to point out that the seemingly small reduction in theoretical frequencies from $\overline{K} = \infty$ to $\overline{K} = 63$ has a large effect on the flutter parameter. As can be seen from table III for panel I, the ratio of $\lambda_{\overline{K}=\infty}/\lambda_{th}$ is 7.3.

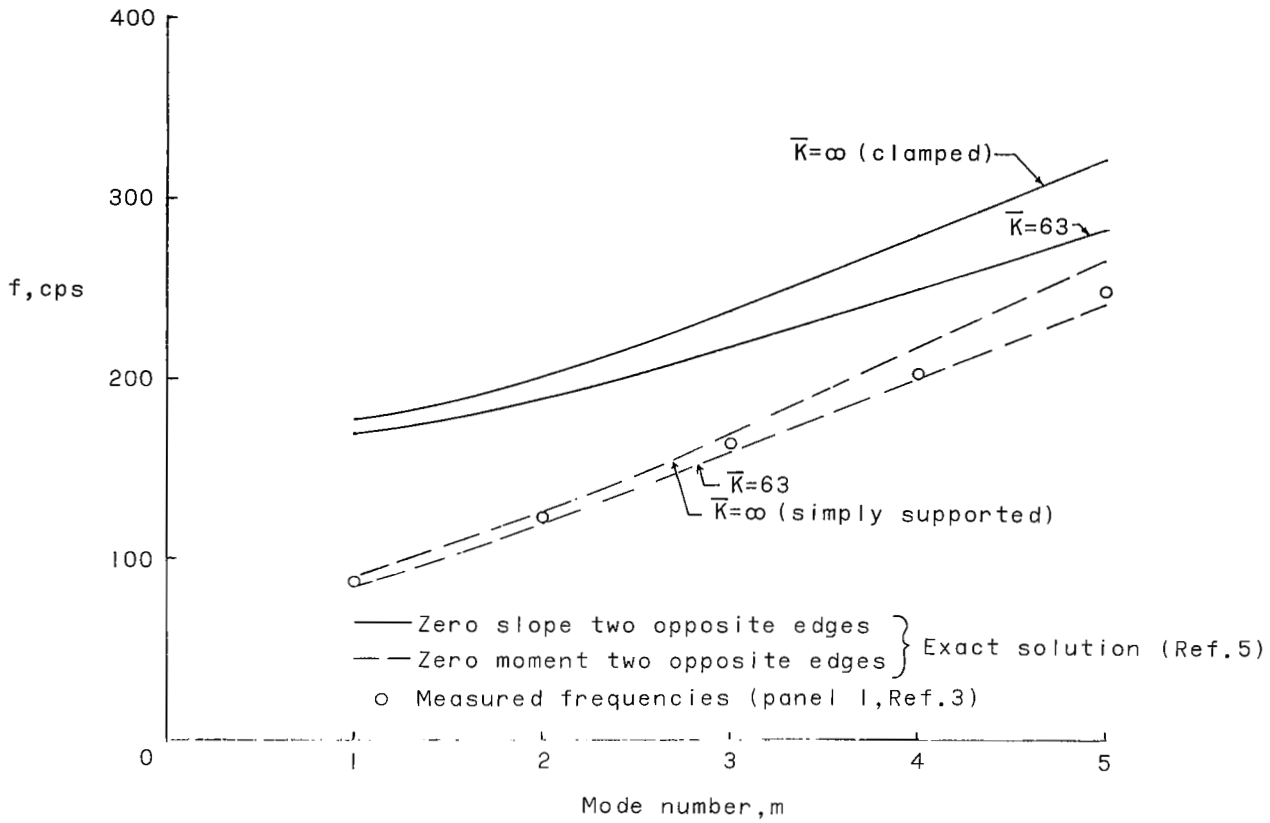

Figure 9.- Comparison of measured frequencies of panel I with theory.

CONCLUDING REMARKS

Corrugation-stiffened panels were tested for flutter in the Langley 9- by 6-foot thermal structures tunnel at Mach 3, dynamic pressures from 1500 psf to 5000 psf (72 to 239 kN/m^2), and stagnation temperatures from 350° F to 660° F (450° to 620° K). The flutter points obtained are presented as a function of panel temperature to show the effects of aerodynamic heating or thermal stress on flutter behavior.

The results from this investigation and some other available experimental data on corrugation-stiffened panels are compared with theory. In order to obtain favorable comparison, it was necessary to account for the deflectional flexibility of the edges at the ends of the corrugations. Even though the edge supports may be rigid, calculations indicate that local distortion of the cross section at the supports can introduce enough flexibility to affect the results significantly. Accounting for the edge effects for the panels tested resulted in as much as three orders of magnitude decrease in the theoretical values of the dynamic pressure parameter. This correction to the theory appears

to account for a large percentage of the discrepancy between theory and experiment. Thus, it is concluded that if attention is given to methods of attaching corrugation-stiffened panels to the substructure to reduce support flexibility, large increases in the dynamic pressure for flutter may be realized.

Langley Research Center,
National Aeronautics and Space Administration,
Langley Station, Hampton, Va., April 20, 1967,
126-14-02-23-23.

APPENDIX A

METHODS FOR CALCULATING DEFLECTIONAL SPRING STIFFNESS K

The panels used in the comparison with theory are categorized into four different support types which are shown in figure 10. Each support type requires a different method for calculation of the equivalent deflectional spring stiffness. Pertinent details of the panel supports are given in table IV.

The first type of support attachment considered corresponds to a panel attached to a rigid support with the corrugations either stamped or crushed to the flat outer skin. (See fig. 10.) The spring effect for this type of support attachment accounts for the loss of panel flexural stiffness near the edges of the corrugations which is caused by the reduction in corrugation depth. Further, the panel span is reduced by $2(c + s)$ to adjust for that portion of the span included in the spring calculations. The deflectional spring stiffness (listed as K_2 in table II) is determined as the ratio of the line load P to

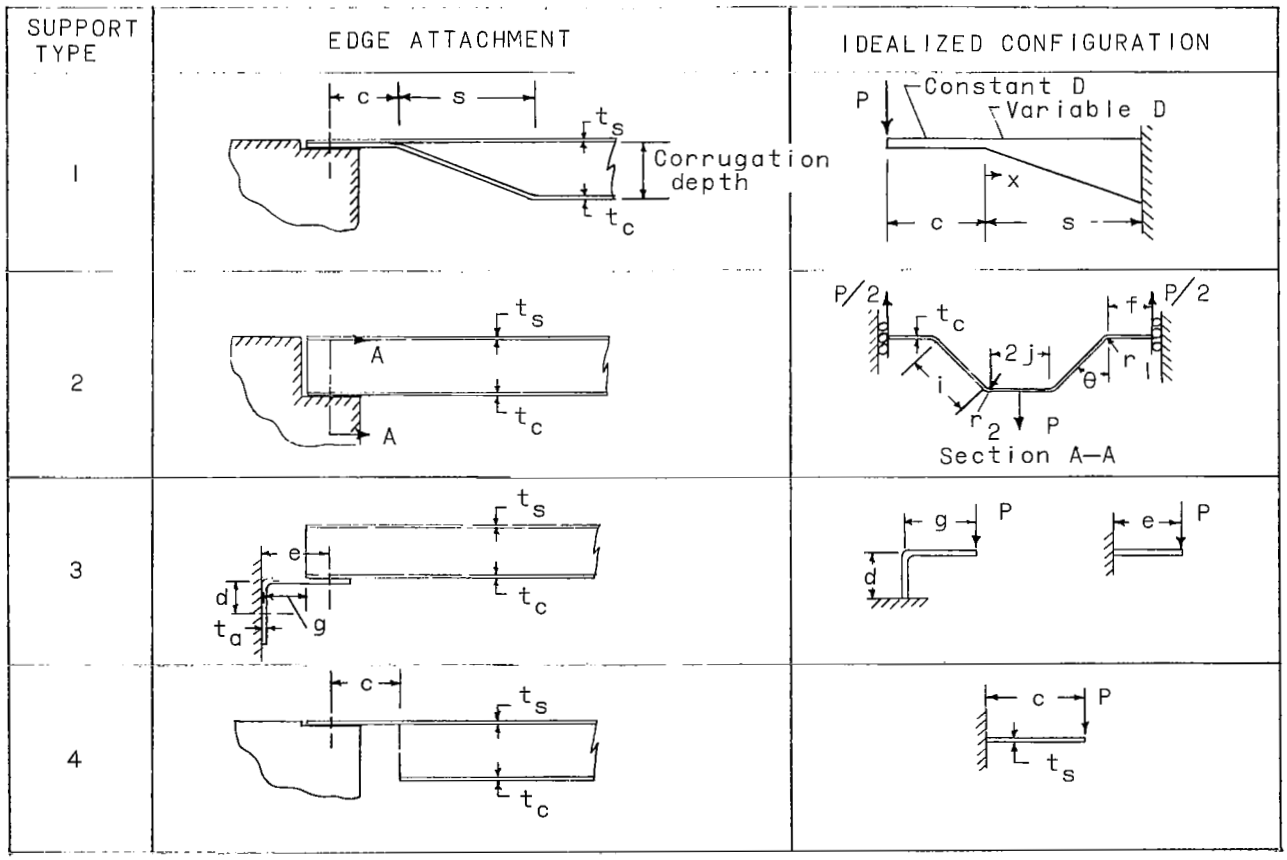

Figure 10.- Actual and idealized support conditions.

the unit deflection at the load for the idealized configuration shown in figure 10. The cubic variation $\left(C_1\left(\frac{x}{s}\right)^3 + C_2\right)$ of the flexural stiffness D over the length s was used where the constant C_2 has the value of D at $x = 0$ and $C_1 + C_2$ has the value of D at $x = s$. For this type of support $K = K_2$.

The second support type shown in figure 10 corresponds to the corrugations extending to and attached to a rigid support. For this type the deflectional flexibility of the corrugation is considered and is analyzed as the idealized configuration shown in figure 10, which represents a segment of a general corrugation. The panels are attached to the rigid structure at a point on the bottom of the corrugations; thus, during vibrations the exposed surface and corrugations may experience relative motion between the exposed skin and the bottom of the corrugations (a breathing effect). This deflectional stiffness (listed as K_1 in table II) is determined by using Castigliano's method (see ref. 15) to find the deflection in the direction of the load P. The boundary conditions are zero horizontal displacement and zero slope at the ends. For this type of support $K = K_1$.

The third support type corresponds to that shown in figure 10 wherein the panel edge is attached to a flexure. The flexure-type support is very common in design where alleviation of thermal stresses is necessary. The flexure, designed as a weak support, may be expected to influence significantly the deflectional stiffness. For this type of support two deflectional stiffnesses are determined and added in series to get the actual stiffness. The deflectional stiffness of the corrugation is obtained in the same manner as was discussed for the type 2 support and again is listed as K_1 in table II; the flexure is treated as a second spring of deflectional stiffness K_2. For the panels listed herein, the value of the spring stiffness of the flexure depends on the direction of the deflectional displacement. The idealized configuration illustrates the pertinent geometry for each direction of displacement. The corresponding spring stiffnesses are used to calculate an equivalent spring stiffness K_2 by the method presented in reference 16.

The fourth support type consists of the attachment of the cover sheet only to a rigid support with the corrugated sheet unsupported as shown in figure 10. The spring stiffness, listed as K_2 in the table, is that of a cantilever beam with a thickness corresponding to that of the cover sheet, and with a length equal to the distance between the unsupported corrugation and the point of attachment of the cover sheet to the support.

APPENDIX B

CONVERSION OF U.S. CUSTOMARY UNITS TO SI UNITS

The International System of Units (SI) was adopted by the Eleventh General Conference on Weights and Measures, Paris, October 1960, in Resolution No. 12 (ref. 6). Conversion factors for the units used herein are given in the following table:

Physical quantity	U.S. Customary Unit	Conversion factor (*)	SI Unit
Length	in.	0.0254	meters (m)
Stiffness	lbf-in.	0.113	joule
Strength	psi = lbf/in^2	6.895×10^3	newtons/meter^2 (N/m^2)
Pressure	lbf/ft^2	47.88	newtons/meter^2 (N/m^2)
Temperature . . .	$^oF + 459.67$	5/9	degrees Kelvin (^oK)

*Multiply value given in U.S. Customary Unit by conversion factor to obtain equivalent value in SI Unit.

Prefixes to indicate multiples of units are as follows:

Prefix	Multiple
mega (M)	10^6
kilo (k)	10^3
centi (c)	10^{-2}
milli (m)	10^{-3}

REFERENCES

1. Kordes, Eldon E.; Tuovila, Weimer J.; and Guy, Lawrence D.: Flutter Research on Skin Panels. NASA TN D-451, 1960.

2. Golden, C. T.; Hager, T. R.; and Sherman, L. L.: Orthotropic Panel Flutter Analysis Correlation. Doc. No. D2-81301 (Contract AF 33(615)-1785), The Boeing Co., 1964.

3. Bohon, Herman L.: Experimental Flutter Results for Corrugation-Stiffened Panels at a Mach Number of 3. NASA TN D-2293, 1964.

4. Bohon, Herman L.; and Dixon, Sidney C.: Some Recent Developments in Flutter of Flat Panels. J. Aircraft, vol. 1, no. 5, Sept.-Oct. 1964, pp. 280-288.

5. Bohon, Herman L.; and Anderson, Melvin S.: Role of Boundary Conditions on Flutter of Orthotropic Panels. AIAA J., vol. 4, no. 7, July 1966, pp. 1241-1248.

6. Mechtly, E. A.: The International System of Units – Physical Constants and Conversion Factors. NASA SP-7012, 1964.

7. Dixon, Sidney C.; Griffith, George E.; and Bohon, Herman L.: Experimental Investigation at Mach Number 3.0 of the Effects of Thermal Stress and Buckling on the Flutter of Four-Bay Aluminum Alloy Panels With Length-Width Ratios of 10. NASA TN D-921, 1961.

8. Bohon, Herman L.: Flutter of Flat Rectangular Orthotropic Panels With Biaxial Loading and Arbitrary Flow Direction. NASA TN D-1949, 1963.

9. Erickson, Larry L.: Supersonic Flutter of Flat Rectangular Orthotropic Panels Elastically Restrained Against Edge Rotation. NASA TN D-3500, 1966.

10. Bohon, Herman L.: Panel Flutter Tests on Full-Scale X-15 Lower Vertical Stabilizer at Mach Number of 3.0. NASA TN D-1385, 1962.

11. Pride, Richard A.; Royster, Dick M.; and Helms, Bobbie F.: Design, Tests, and Analysis of a Hot Structure for Lifting Reentry Vehicles. NASA TN D-2186, 1964.

12. Weidman, Deene J.: Experimental Flutter Results for Corrugation-Stiffened and Unstiffened Panels. NASA TN D-3301, 1966. (Errata 1, Oct. 1967.)

13. Stroud, W. Jefferson: Elastic Constants for Bending and Twisting of Corrugation-Stiffened Panels. NASA TR R-166, 1963.

14. Gaspers, Peter A., Jr.; and Redd, Bass: A Theoretical Analysis of the Flutter of Orthotropic Panels Exposed to a High Supersonic Stream of Arbitrary Direction. NASA TN D-3551, 1966.

15. Wang, Chu-Kia: Statically Indeterminate Structures. McGraw-Hill Book Co., Inc., c.1953.

16. Semonian, Joseph W.; and Anderson, Roger A.: An Analysis of the Stability and Ultimate Bending Strength of Multiweb Beams With Formed-Channel Webs. NACA TN 3232, 1954.

TABLE I

SUMMARY OF FLUTTER CONDITIONS

Panel	Test	T_t		Start of flutter											End of flutter										
				q		Δp		ΔT_1		ΔT_2		ΔT_3		f_f, cps	q		Δp		ΔT_1		ΔT_2		ΔT_3		f_f, cps
		^oF	^oK	psf	$\frac{kN}{m^2}$	psi	$\frac{kN}{m^2}$	^oF	^oK	^oF	^oK	^oF	^oK		psf	$\frac{kN}{m^2}$	psf	$\frac{kN}{m^2}$	^oF	^oK	^oF	^oK	^oF	^oK	
IIIa	1	400	478	2970	142	0.06	0.41	No flutter test																	
IIIa	2	500	534	4250	204	-.02	-.14	145	80	90	50	3	1.7	113											
IIIa	3	550	560	4620	221	-.22	-1.51	105	58	69	38	0	0	115											
IIIa	4	360	455	4700	225	.28	1.93	108	60	73	41	2	1.1	116											
IIIb	5	600	589	4600	220	-.38	-2.62	88	49	60	33	0	0	115	4900	235	-0.22	-1.51	338	189	303	168	28	16	120
IIIb	6	500	534	4450	213	-.44	-3.03	115	64	70	39	0	0	113	3810	183	-.05	-.33	234	130	196	109	7	3.9	112
				*4100	196	-.16	-1.10	266	148	230	128	13	7.2	115											
IIIb	7	350	450	4840	232	.36	2.48	80	44	49	27	0	0	114	**3730	179	-.10	-.69	135	75	130	72	12	6.7	112
				4200	201	-.25	-1.72	133	74	130	72	23	13	110	**4440	212	-.05	-.33	122	68	124	69	35	19	112
IVa	1	400	478	3210	154	-.10	-.69	---	---	174	96	7	3.9	390	**2940	141	-.11	-.76	---	---	191	106	19	11	390
IVa	2	400	478	3970	190	0	0	---	---	111	62	0	0	200											
IVb	3	400	478	3200	153	-.12	-.83	---	---	153	85	3	1.7	250											
IVb	4	540	556	4450	213	.12	.83	---	---	114	63	0	0	345	2250	108	.06	.41	---	---	276	153	23	13	330
				*2640	126	.25	1.72	---	---	290	161	36	20	193	1930	93	.07	.48	---	---	304	169	66	37	180
				*2360	113	.26	1.79	---	---	306	170	82	46	183	2040	98	.04	.29	---	---	311	173	99	55	170
				*2170	108	.22	1.51	---	---	312	173	118	66	175	1840	88	.04	.29	---	---	313	174	132	73	163
IVb	5	550	560	3980	191	.22	1.51	---	---	88	49	0	0	225	**1980	95	-.15	-1.03	---	---	222	123	6	3.3	170
				*2080	100	-.02	-.14	---	---	234	130	15	8.3	190	2070	99	-.17	-1.17	---	---	260	144	36	20	141
				*3430	164	-.03	-.21	---	---	267	148	56	31	161	2540	122	-.15	-1.03	---	---	267	148	88	49	145
V	1	450	505	2020	97	-.17	-1.17	125	69	80	44	0	0	125											
V	2	400	478	1530	73	-.25	-1.72	135	75	105	58	5	2.8	122											
V	3	350	450	2520	121	-.35	-2.41	95	53	70	39	0	0	125											

*Panel thermally buckled when flutter started.

**Panel flat when flutter stopped.

TABLE II

DETAILS OF CORRUGATION-STIFFENED FLUTTER PANELS

Panel	Reference	Support type	Panel length, a		Panel width, b		E		D_1		D_2		D_{12}		K_1		K_2		K		$\overline{K}$
			in.	m	in.	m	psi	$\frac{GN}{m^2}$	lb-in.	N-m	lb-in.	N-m	lb-in.	N-m	$\frac{lb/in.}{in.}$	$\frac{MN/m}{m}$	$\frac{lb/in.}{in.}$	$\frac{MN/m}{m}$	$\frac{lb/in.}{in.}$	$\frac{MN/m}{m}$	
B9	10	1	18.30	0.465	*8.00	0.203	31×10^6	214	87.1	9.8	23,178	2620	8,324	940	----	---	590	4.1	590	4.1	0.4
C	11	2	24.50	.623	24.50	.623	31	214	14.2	1.6	21,679	2450	6,550	740	344	2.4	-----	---	344	2.4	7.5
I	3	3	23.82	.605	23.82	.605	31	214	9.1	1.0	14,545	1640	3,315	376	2582	17.8	11,100	76.5	2100	14.5	63.0
II	3	3	23.82	.605	23.82	.605	31	214	8.3	.94	36,725	4150	7,068	798	618	4.2	11,100	76.5	585	4.0	6.9
III	Present paper	3	23.82	.605	23.82	.605	32	220	20.9	2.4	18,860	2130	4,413	500	5856	40.4	11,400	78.5	3870	26.6	89.0
IV	Present paper	3	19.00	.483	19.00	.483	28	193	7.7	.87	29,894	3380	4,944	556	285	2.0	10,000	68.9	278	1.9	2.1
V	Present paper	3	19.00	.483	19.00	.483	28	193	7.7	.87	33,707	3800	5,726	646	558	3.8	305	2.1	197	1.4	2.6
U-1	12	4	24.00	.61	24.00	.61	10	69	3.1	.35	1,800	204	457	52			20	.14	20	.14	5.0
U-2	12	4	24.00	.61	24.00	.61	31	214	9.1	1.03	14,545	1640	3,315	376			82	.56	82	.56	2.5
V-1	12	4	24.00	.61	24.00	.61	10	69	16.9	1.9	19,337	2180	3,041	344			144	1.0	144	1.0	5.4
V-2	12	4	24.00	.61	24.00	.61	31	214	12.9	1.46	31,494	3560	8,541	464			82	.56	82	.56	1.2
V-3	12	4	24.00	.61	24.00	.61	28	193	9.4	1.06	27,603	3120	7,461	842			60	.41	60	.41	1.0
V-4	12	4	24.00	.61	24.00	.61	31	214	47.9	5.4	48,000	5420	10,514	1190			362	2.5	362	2.5	3.4
V-5	12	4	24.00	.61	24.00	.61	10	69	21.2	2.4	17,339	1960	3,827	433			160	1.1	160	1.1	4.1
V-6	12	4	24.00	.61	24.00	.61	30	206	47.5	5.36	56,942	6420	8,949	1020			412	2.8	412	2.8	3.2
H-1	12	4	24.00	.61	24.00	.61	31	214	8.3	.94	36,725	4150	7,068	798			62	.43	62	.43	.8
S-1	12	1	37.30	.946	*17.40	.441	31	214	10.2	1.15	23,875	2700	7,592	856			197	1.35	197	1.35	1.4
S-2	12	1	37.30	.946	*16.10	.408	31	214	10.5	1.19	47,266	5350	15,540	1760			171	1.18	171	1.18	.5
S-3	12	1	37.30	.946	*16.10	.408	31	214	11.1	1.25	44,762	5060	15,927	1800			169	1.16	169	1.16	.5
S-4	12	1	37.30	.946	*16.10	.408	31	214	11.8	1.33	42,477	4790	16,251	1840			166	1.14	166	1.14	.5
S-5	12	1	37.30	.946	*17.40	.441	31	214	9.0	1.02	27,101	3060	7,083	800			204	1.4	204	1.4	1.3
S-6	12	1	37.30	.946	*17.40	.441	10	69	2.9	.33	8,742	987	2,285	258			66	.45	66	.45	1.3
S-7	12	1	37.30	.946	*17.40	.441	10	69	3.3	.37	7,702	870	2,449	277			64	.44	64	.44	1.4
S-8	12	1	37.30	.946	*16.10	.408	31	214	8.3	.94	60,351	6800	13,464	1520			185	1.27	185	1.27	.4
S-9	12	1	37.30	.946	*16.10	.408	10	69	2.7	.31	19,468	2200	4,343	490			60	.41	60	.41	.4
S-10	12	1	37.30	.946	*16.10	.408	31	214	4.2	.47	48,363	5460	10,703	1210			107	.74	107	.74	.3

*Panel width reduced by $2(c + s)$ (see fig. 10).

TABLE III

COMPARISON OF THEORY AND EXPERIMENT

Panel	Reference	Mach number	$\overline{K}$	Experiment	Theory (ref. 5)	
				λ_{cr}	$\frac{\lambda_{th}}{\lambda_{cr}}$	$\frac{\lambda_{\overline{K}=\infty}}{\lambda_{cr}}$
B9	10	3.0	0.4	1,730	1.88	63.0
C	11	1.87	7.5	18,700	.72	25.4
I	3	3.0	63.0	25,900	1.85	13.5
II	3	3.0	6.9	24,700	.92	50.0
III	Present paper	3.0	89.0	18,100	2.48	8.8
IV	Present paper	3.0	2.1	25,700	.33	23.1
V	Present paper	3.0	2.6	38,300	.30	19.3
U-1	12	2.83	5.0	5,600	1.19	15.5
U-2	12	1.96	2.5	2,310	2.60	151.0
V-1	12	1.63	3.4	4,560	1.73	25.7
V-2	12	1.96	1.2	5,210	.67	161.0
V-3	12	1.72	1.0	3,250	1.08	334.0
V-4	12	1.63	3.4	4,750	1.41	33.5
V-5	12	1.63	4.1	2,100	3.57	55.6
V-6	12	1.63	3.2	3,740	2.06	33.7
H-1	12	1.63	.8	4,590	.81	208.0
S-1	12	1.57	1.4	22,600	1.85	430.0
S-2	12	1.57	.5	25,400	1.19	1340.0
S-3	12	1.85	.5	46,400	.62	700.0
S-4	12	1.85	.5	33,700	.80	910.0
S-5	12	2.1	1.3	39,200	1.27	270.0
S-6	12	2.1	1.3	44,000	1.05	241.0
S-7	12	1.57	1.4	63,500	.67	153.0
S-8	12	2.1	.4	45,000	.78	863.0
S-9	12	2.1	.4	21,600	1.60	1790.0
S-10	12	1.57	.3	95,600	.53	812.0

TABLE IV

DETAILS OF CORRUGATION-STIFFENED PANEL SUPPORTS

Panel	Support type	c		d		e		f		g		i		j		r_1		r_2		θ, deg	s		t_a		t_c		t_s	
		in.	mm	in.	mm	in.	mm	in.	mm	in.	mm	in.	mm	in.	mm	in.	mm	in.	mm		in.	mm	in.	mm	in.	mm	in.	mm
B9	1	0.563	14.30																		1.70	43.1	----	----	0.012	0.305	0.030	0.762
C	2	----	----	---	---	---	---	0.25	6.35	0.05	1.27	0.50	12.7	0.25	6.35	0.032	0.814	0.032	0.814	30	---	---	----	----	.0107	.272	.0107	.272
I	3	----	----	0.38	9.65	0.38	9.65	.25	6.35	.05	1.27	.125	3.18	.25	6.35	.02	.508	.25	6.35	0	---	---	0.032	0.814	.010	.254	.010	.254
II	3	----	----	.38	9.65	.38	9.65	.25	6.35	.05	1.27	.50	12.7	.25	6.35	.02	.508	.02	.508	0	---	---	.032	.814	.010	.254	.010	.254
III	3	----	----	.38	9.65	.38	9.65	.25	6.35	.05	1.27	.125	3.18	.25	6.35	.026	.66	.25	6.35	0	---	---	.032	.814	.013	.330	.013	.330
IV	3	----	----	.38	9.65	.38	9.65	.25	6.35	.05	1.27	.50	12.7	.25	6.35	.016	.406	.016	.406	0	---	---	.032	.814	.008	.203	.012	.305
V	3	----	----	.38	9.65	.38	9.65	.25	6.35	.05	1.27	.50	12.7	.25	6.35	.02	.508	.02	.508	0	---	---	.010	.254	.010	.254	.010	.254
U-1	4	.5	12.7																		---	---	----	----	.01	.254	.01	.254
U-2	4	.5	12.7																		---	---	----	----	.011	.280	.011	.280
V-1	4	.5	12.7																		---	---	----	----	.019	.483	.02	.505
V-2	4	.5	12.7																		---	---	----	----	.011	.280	.011	.280
V-3	4	.5	12.7																		---	---	----	----	.01	.254	.01	.254
V-4	4	.5	12.7																		---	---	----	----	.018	.457	.018	.457
V-5	4	.5	12.7																		---	---	----	----	.02	.508	.02	.508
V-6	4	.5	12.7																		---	---	----	----	.019	.483	.019	.483
H-1	4	.5	12.7																		---	---	----	----	.01	.254	.01	.254
S-1	1	.5	12.7																		1.4	35.5	----	----	.01	.254	.01	.254
S-2	1	.5	12.7																		2.0	50.8	----	----	.01	.254	.01	.254
S-3	1	.5	12.7																		2.0	50.8	----	----	.01	.254	.01	.254
S-4	1	.5	12.7																		2.0	50.8	----	----	.01	.254	.01	.254
S-5	1	.5	12.7																		1.4	35.5	----	----	.01	.254	.01	.254
S-6	1	.5	12.7																		1.4	35.5	----	----	.01	.254	.01	.254
S-7	1	.5	12.7																		1.4	35.5	----	----	.01	.254	.01	.254
S-8	1	.5	12.7																		2.0	50.8	----	----	.01	.254	.01	.254
S-9	1	.5	12.7																		2.0	50.8	----	----	.01	.254	.01	.254
S-10	1	.5	12.7																		2.0	50.8	----	----	.005	.203	.005	.203